Terrestrial Photosynthetic Light-use Efficiency of Temperate Ecosystems Can Be Inferred from Space.

Thomas Hilker[1,*], Nicholas C. Coops[1], Forrest G. Hall[2,3], Caroline J. Nichol[4], Alexei Lyapustin[2,3], T. Andrew Black[5], Michael A. Wulder[6], Ray Leuning[7], Alan Barr[8], David Y. Hollinger[9], Bill Munger[10], Compton J. Tucker[3]

[1]Faculty of Forest Resources Management, University of British Columbia, 2424 Main Mall, Vancouver, BC, Canada.

[2]Joint Center for Earth Systems Technology, University of Maryland, Baltimore County, USA

[3]NASA Goddard Space Flight Center, Greenbelt Maryland, 20771, USA, Code 614.4

[4]School of GeoSciences, University of Edinburgh, West Mains Road, Edinburgh EH9 3JN, Scotland UK

[5]Faculty of Land and Food Systems, University of British Columbia, 2357 Main Mall, Vancouver, BC, Canada.

[6]Canadian Forest Service, 506 West Burnside Road, Victoria, BC, Canada

[7]CSIRO Marine and Atmospheric Research, Canberra, Australia

[8]Environment Canada, 11 Innovation Blvd., Saskatoon, SK, Canada

[9]US Forest Service, Northeast Research Station, 271 Mast Rd, Durham, New Hampshire

[10]Harvard University, Cambridge, MA, USA

Pre-print of published version:
Hilker, T., Coops, N.C., Hall, F.G., Nichol, C.J, Lyapustin, A., Black, T.A., Wulder, M.A., Leuning, R., Barr, A., Hollinger, D.Y., Munger, J. W., Tucker, C. J. (2011) Terrestrial Photosynthetic Light-use Efficiency of Temperate Ecosystems Can Be Inferred from Space. *Journal of Geophysical Research - Biogeosciences*, doi:10.1029/2011JG001692, in press.

[1] * corresponding author: Phone: ~~+1 (604) 827 4429, Fax :+1 (604) 822 9106, thomas.hilker@ubc.ca~~

Current address: thomas.hilker@nasa.gov

Abstract

Terrestrial ecosystems absorb about 2.8 Gt C yr^{-1}, which is estimated to be about a quarter of the carbon emitted from fossil fuel combustion. However, the uncertainties of this sink are large, in the order of ± 40%, with spatial and temporal variations largely unknown. One of the largest factors contributing to the uncertainty is photosynthesis, the process by which plants absorb carbon from the atmosphere. Currently, photosynthesis, or gross ecosystem productivity (GEP), can only be inferred from flux-towers by measuring the exchange of CO_2 in the surrounding air column. Consequently, carbon models suffer from a lack of spatial coverage of accurate GEP observations. Here, we show that photosynthetic light-use efficiency (ε), hence photosynthesis can be directly inferred from spaceborne measurements of reflectance. We demonstrate that the differential between reflectance measurements in bands associated with the vegetation xanthophyll cycle and estimates of canopy shading obtained from multi-angular satellite observations (using the CHRIS/Proba sensor) permits us to infer plant photosynthetic efficiency, independently of vegetation type and structure (r^2=0.68, compared to flux measurements). This is a significant advance over previous approaches seeking to model global scale photosynthesis indirectly from a combination of growth limiting factors, most notably pressure deficit and temperature. When combined with modeled global scale photosynthesis, satellite inferred ε can improve model estimates through data assimilation. We anticipate that our findings will guide the development of new spaceborne approaches to observe vegetation carbon uptake and improve current predictions of global CO_2 budgets and future climate scenarios by providing regularly timed calibration points for modeling plant photosynthesis consistently at a global scale.

1. Introduction

The net carbon exchange of terrestrial ecosystems is dominated by GEP and respiration [*Valentini et al.*, 2000], both of which are in the order of about 60 Gt year^{-1}. GEP is the product of photosynthetically active radiation (PAR) incident upon the canopy, the fraction of it being absorbed by photosynthetically active vegetation elements (green f_{PAR} *referred to herin as* f_{PAR}) and the efficiency (ε) with which plants can use this absorbed radiation energy to produce biomass [*Monteith*, 1977]. While f_{PAR} and PAR can be readily determined from remote sensing observations globally [*Myneni and Williams*, 1994; *Sellers et al.*, 1994; *Van Laake and Sanchez-Azofeifa*, 2005], direct inference of ε has not yet been possible [*Hilker et al.*, 2008a; *Rahman et al.*, 2001]. Light-use efficiency is determined by the most limiting of a large number of variables restraining the photochemical reaction process and, as a result, varies widely both in space and time. Under optimal conditions, most of the absorbed radiation energy will be directed towards the reaction center of Photosystem (PS) II, where it is used to produce photosynthate by fixing CO_2 from the surrounding air column. When photosynthesis is limited by water availability, nutrients or temperatures, excess radiation energy is dissipated thermally by means of protective leaf pigments: Triggered by the acidification of the thylakoid membrane, the xanthophyll cycle pigment violaxanthin is converted rapidly via intermediate antheraxanthin to zeaxanthin [*Demmig- Adams and Adams*, 1996]. This process is reversed when light limits photosynthesis [*Demmig- Adams and Adams*, 1996, *Demmig-Adams*, 1998].

Remote sensing of GEP and hence ε in a spatially contiguous mode has been a long term goal of Earth and climate change research seeking universal, generic modelling approaches of plant productivity applicable across multiple biomes and a wide variety of vegetation types. Numerous studies [*Fuentes et al.*, 2006; *Gamon et al.*, 1992; *Gamon et al.*, 1997; *Meroni et al.*, 2008, *Nichol et al.*, 2000] have related ε

to the photochemical reflectance index (PRI), a narrow waveband spectral index that is directly associated with changes in the xanthophyll cycle, but the dependency of PRI on extraneous effects such as canopy structure, reflectance from non-photosynthetic background, the ratio of chlorophyll to carotenoid content [*Stylinski et al.,* 2002; *Nakaji et al.,* 2006] and the sun-observer geometry have hampered its use at canopy, landscape and global scales for almost two decades. At the leaf scale, non-photochemical quenching is primarily a function of the degree of leaf illumination [*Demmig-Adams*, 1998]: In cases where GEP is limited by factors other than light ($\varepsilon < \varepsilon_{max}$), ε is closely related to canopy shadow fractions (α_s) [*Hall et al.*, 2008; *Hilker et al.*, 2008b; *Hilker et al.*, 2008c]. This is due to the fact that sunlit leaves are more likely to be exposed to excess radiation levels than shaded leaves. However, this relationship disappears under conditions where light is limiting GEP ($\varepsilon_{canopy} = \varepsilon_{max}$), as in this case, photosynthesis will, by definition, not be down-regulated in either sunlit or shaded leaves ($\varepsilon_{sunlit} = \varepsilon_{shaded} = \varepsilon_{max}$). As a result, the slope of the relationship between ε and α_s is proportional to canopy light-use efficiency [*Hall et al.*, 2008, 2011; *Hilker et al.*, 2010].

This concept has two important implications for remote sensing of ε using PRI. First, stand level ε cannot be observed from traditional, mono-angle observations, because the proportion of α_s observed by the sensor at a given time may not be representative of the canopy and the contribution of α_s to the photosynthetic down-regulation is unknown. Second, multi-angular measurements of PRI can be used to determine stand-level ε, if α_s is known for each view angle. This second proposition is true, because under the assumption of singular leaf scattering, which is reasonable for remote sensing of wavelengths in the visible bands, a normalized difference reflectance index cannot change its value with the viewing geometry unless the value of one of its bands changes as a physiological response of the degree of leaf illumination [*Hall et al.*, 2008]. Based on these two principles it can be concluded that the first derivative of PRI with respect to shadow fractions ($\Delta PRI\ \Delta\alpha_s^{-1}$ or PRI') can be used to infer instantaneous ε at the canopy level [*Hilker et al.*, 2010].

In this paper, we demonstrate our approach, which has been shown analytically in *Hall et al.* [2011], from space using multi-angular, satellite observations acquired by the CHRIS (Compact High Resolution Imaging Spectrometer) sensor onboard European Space Agency's PROBA (Project for On-Board Autonomy) research satellite. The objective of this study was to compare spaceborne measurements of PRI' with eddy covariance (EC) observations of ε acquired across a number of forest types with different structure and physiology, and to demonstrate the usability of PRI' as a generic technique for inferring ε across these different biomes from satellite data.

2. Site Description

To demonstrate the robustness of our approach, eight different sites were selected based on the availability of simultaneous CHRIS/Proba satellite data and eddy-flux tower observations. Although data were not available for some important ecosystems such as tropical sites, the ecosystems that were sampled cover a wide range of forest age classes and temperate ecosystem types from boreal needle-leaf to wet-temperate eucalypt forests; an overview and site description is given in Table 1. Figure 1 shows a map of the various site locations, the structural differences of the test sites used in this study are illustrated in Figure 2. The forest structure across the different sites ranged from recent regeneration planted after harvest (HJP2002) to mature, coniferous (e.g. DF-49) and broadleaf (e.g. Harvard) forest stands. The figure also illustrates the different stand densities and associated background reflectance visible from optical data, which is lower for the denser forest stands (e.g. Fig 2A and B), but higher especially in case of Figure D, G and H.

3. Methods

3.1 Eddy flux observations

Canopy GEP was determined from eddy-covariance data acquired from the data archive of the Canadian Carbon Program (CCP) for the Canadian sites, Ameriflux for the US sites, and Ozflux for the Australian site (Table 1). Net ecosystem exchange (NEE) was determined as the sum of the half-hourly fluxes of CO_2 and the rate of change in CO_2 storage in the air column between ground and EC-measurement level [*Barr et al.*, 2004]. In case of the Harvard and Tumbarumba sites, fluxes were available as hourly observations [*Horii et al.*, 2004; *Leuning et al.*, 2005]. Incident and reflected PAR [μmol m^{-2} s^{-1}] was measured from upward and downward looking quantum sensors above and below the canopy and f_{PAR} was derived at each site from the incident and reflected total PAR measured above and below the canopy ($\rho_1(\theta)$ and $\rho_2(\theta)$), the effective leaf area index (L_e), and the solar zenith angle (θ) at the time of measurement [*Chen*, 1996; *Chen et al.*, 2006].

$$f_{PAR} = \left(1-\rho_1(\theta)\right) - \left(1-\rho_2(\theta)\right)e^{\left(\frac{G_t(\theta)LAI_e}{\cos\theta}\right)} \qquad (1)$$

where $G_t(\theta)$ is the projection coefficient for total PAR transmission, approximated as a constant of 0.5. (Please note that this an approximation, as f_{PAR} refers to "green f_{PAR}" [*Chen*, 1996]).

Gross ecosystem production was determined as the difference between net ecosystem exchange (NEE) and daytime ecosystem respiration (R_D) [*Humphreys et al.*, 2006]. R_D was calculated using the annual exponential relationship between nighttime NEE and soil temperature at 5-cm depth after applying a logarithmic transformation to correct for heteroscedasticity [*Black et al.*, 1996; *Goulden and Crill*, 1997]. Finally, ε as defined in *Monteith* [1972; 1977], can be described as the ratio of the photosynthetic net output (GEP) divided by the energy input into the photosynthetic system:

$$\varepsilon = \frac{GEP}{PAR \times f_{PAR}} \qquad (2)$$

More detailed descriptions on processing of the eddy-covariance data can be found for instance in *Humphreys et al.*, [2006]; *Leuning et al.*, [2005], a comprehensive review on fluxnet procedures and processing of EC-data is provided in *Baldocchi et al.*,[2001].

3.2 CHRIS/Proba imagery

CHRIS is an imaging spectrometer with a 615 km sun-synchronous orbit and an orbital repeat cycle of approximately 7 days. Its maximum spatial resolution is 18 m or 34 m at nadir, depending on the mode setting, with a swath width of 14 km. The CHRIS/Proba configuration permits along-track narrow-band spectrometric observations of PRI of up to five angles (+55˚, +36˚, 0˚,–36˚,–55˚). This data is acquired nearly simultaneously within each overpass during which stand level ε may be considered constant. As a demonstration instrument, CHRIS/Proba provides areal coverage for a limited number of pre-defined sites [*Fletcher*, 2004]. CHRIS/Proba images obtained from ESA's online archive (https://oa-es.eo.esa.int/ra/) were acquired between 2001 and 2009.

Acquisitions having simultaneous EC-flux data were selected to represent as wide a range of different structural types as possible to evaluate the ecosystem robustness of the concept. No available observations were excluded from this analysis. CHRIS data can be acquired in different modes to allow data collection with variable wavebands and bandwidths. For this study, CHRIS data collected in modes 1 and 3 were used, as they provided the appropriate PRI wavebands at around 531 and 570 nm. The satellite observations were pre-processed using the VISAT tool of the European Space Agency to reduce data noise [*Gomez-Chova et al.*, 2008], convert satellite measured radiance to top of atmosphere reflectance and screen the images for clouds [*Thuillier et al.*, 2003].

Satellite observed reflectance depends on two main parameters, aerosol optical thickness (AOT) and the bi-directional reflectance function (BDRF). Appropriate algorithms to deal accurately and

simultaneously with both BDRF and the effects of aerosols on path scattering have yet to be developed for CHRIS/Proba. Most commonly a Lambertian surface model is used [*Hilker et al.*, 2009]. While this step simplifies processing, the Lambertian assumption reduces anisotropy of derived surface reflectance with the error dependent on the viewing geometry [*Lyapustin et al.*, 2007]. *Hilker et al.* [2009] showed that this assumption directly contradicts the multi-angle effects observed in PRI and consequently, no meaningful multi-angular observations of PRI can be obtained from single orbit atmospheric corrections [Hilker et al., 2009]. Our previous work has also demonstrated that this challenge could be overcome when using multiple acquisitions over time for which the retrieval of aerosol optical thickness does not require these simplifying assumptions [*Hilker et al.*, 2009; *Lyapustin et al.*, 2007]; however, no such algorithm currently exists for CHRIS/Proba. From theoretical considerations, it can be shown that the error associated with atmospheric effects is mostly a function of the range of shadow fractions viewed during an overpass. *Hall et al.*, 2011 showed that aerosols tend to suppress the variation of PRI with shadow fraction, hence modify the relationship with LUE and further demonstrated that the PRI' – LUE relationship remains robust in spite of it. Clearly an improved atmospheric correction technique for CHRIS/Proba should further improve the relationships by mitigating atmospheric noise .

Another critical issue for the use of CHRIS/Proba observations is geometric correction of the multi-angular data. First, images captured at large view angles are susceptible to resolution change and blurring, which makes the precise location of ground control points (GCPs) difficult, and second, local geometric distortion caused by topographic effects and/or platform instability can make rigid transformation models unreliable [*Ma et al.*, 2010]. Arguably, the most rigid approach for image registration at off-nadir angles are physical sensor models [*Leprince et al.*, 2007; *Toutin*, 2004], however, these models require reliable metadata on sensor-target geometry which are not available for CHRIS/Proba [*Shaker et al.*, 2008]. To compensate for this lack of information, we applied a two step geo-rectification algorithm described in *Ma et al.*, [2010] and registered CHRIS/Proba satellite imagery

with respect to Landsat observations of the same locations. First, common ground control points (GCPs) between Landsat and CHRIS/Proba were automatically identified using a scale-invariant feature transform (SIFT) [*Lowe*, 2004]. SIFT is a method for extracting and matching distinctive features in image pairs invariant to image scale and rotation, across a substantial range of affine distortion, change in 3D viewpoint, addition of noise, and change in illumination [*Lowe*, 2004]. The network of these initial GCPs was then densified in a second step using a normalized cross correlation (NCC) approach and CHRIS/Proba images were warped by means of a non-reflective similarity transformation [*Goshtasby*, 1988]. For moderately undulated terrain, such as the case for most eddy-covariance flux sites [*Baldocchi et al.*, 2001], this simple approach has been shown to yield geo-location accuracies within the sub-pixel range which should be sufficiently accurate for stand level observations [*Ma et al.*, 2010] given the spatial resolution of the CHRIS/PROBA data.

3.3 Computation of PRI'

In previous studies [*Hall et al.*, 2008; *Hilker et al.*, 2009; *Hilker et al.*, 2010] canopy shadow fractions have been estimated from airborne light detection and ranging (LiDAR). While this approach has proven suitable to provide accurate measurements of mutual shading of individual stands [*Hilker et al.*, 2008b], the availability of LiDAR is limited, and, consequently global estimates of PRI' will require alternative retrievals of α_s. One possibility is to derive α_s directly from the satellite imagery using spectral mixture analysis [*Hall et al.*, 1997,1996,1995; *Peddle and Smith*, 2005] thereby avoiding the need for a secondary data source. This technique also has the advantage that it only considers the shading associated with PRI. Various algorithms are available for spectral unmixing; in this study we used the sequential maximum angle convex cone (SMACC) model [*Gruninger et al.*, 2004]. The model defines spectral endmembers as vectors within a data set that cannot be represented by a positive linear combination of

other vectors. An advantage of SMACC is that, as a non-supervised classification technique, it allows automated extraction of canopy shading. To avoid overfitting the model, two endmembers (sunlit leaves, sunlit background) were derived per CHRIS/Proba scene, in addition to α_s (Please note that shaded background was not explicitly extracted, as the PRI values as obtained from CHRIS/Proba are also a composite of leaf and background reflectance). Shadow fractions were derived on a pixel-by-pixel basis for each image.

PRI was computed from CHRIS/Proba imagery as the normalized difference of CHRIS bands 4 (529 nm, Bandwidth: 12.9 nm) and 6 (569 nm, Bandwidth: 14.1 nm) for images acquired in CHRIS Mode 3 (all sites except for the southern BOREAS region), and band 11 (532 nm, Bandwidth 13.4 nm) and 15 (573 nm, Bandwidth 9.6 nm) for images acquired in CHRIS Mode 1 [*Gamon et al.*, 1992]. PRI and corresponding α_s were computed for each pixel of a multi-angular image stack acquired during one overpass (see Figure 3). A single value of PRI' was derived from a simple linear regression model [*Hilker et al.,* 2010] for each overpass. In order to compare PRI' to EC derived ε, PRI' observations were then averaged in a radius of 150 m around the tower and half hourly ε was computed for each satellite overpass (satellite noon ±15 minutes).

4. Results

In total, images from 51 CHRIS/Proba overpasses were acquired across all different sites with up to 5 cloud free, multi-angular observations per overpass. The light-use efficiency determined from the eddy covariance systems ranged from 0.01 g CMJ^{-1} to 0.96 g CMJ^{-1} across all different sites, Figure 4 shows a summary of EC-derived ε observed during all CHRIS/Proba overpasses (satellite noon ±15 minutes). Highest values of ε were observed for the Harvard and DF-49 sites, whereas ε was lowest at the

harvested Jack pine site (HJP 2002). These observations of the instantaneous LUE at the satellite overpass time likely differ from the average diurnal physiological conditions of each stand.

Significant relationships were found between PRI and α_s across all sites; when observed under low levels of ε, the average coefficient of determination was r^2=0.76 ($p<0.01$, $\varepsilon<0.05$ $gCMJ^{-1}$). As theory predicts, the dependence of ε on α_s weakened with increasing ε, as PRI of sunlit and shaded canopy were more nearly equal. For instance, the mean coefficient of determination was r^2=0.21 for ε>0.25; a summary of the strength of the relationship between PRI and α_s across all sites is given in Figure 5. Figure 6 illustrates the slope between PRI and α_s for four different levels of ε, using the HJP 1975 site as an example, and contrasts these observations with potential canopy stress factors, notably pressure deficit (D) and temperature (T), observed from micro-meteorological data (Figures E-H). The figure demonstrates the link between PRI' and environmental conditions. For instance, the slope between PRI and α_s was steepest when the physiological stress factors were highest (high D and T, Figure A and E). Only a moderate slope was found under a more relaxed state of the xanthophyll cycle (higher ε), while the relationship between PRI and α_s began to disintegrate (Fig D). The figure also illustrates the correspondence between D, T, and PAR as major environmental factors on one side, and GEP as the physiological response on the other.

The relationship between PRI' and ε derived from eddy-covariance towers across all study sites is shown in Figure 7. Each data point represents the slope between PRI and α_s observed during one overpass (up to 5 different view angles). A strong, logarithmic relationship was found between EC-derived ε and PRI' obtained from the CHRIS/Proba imagery (r^2=0.68, $p<0.01$). Despite the notable differences in structure, species composition, climate and location, all observations followed the same non-linear function derived theoretically in Hall et al, 2008 that showed this relationship to be insensitive to the unstressed reflectance and structure of the vegetation, including background, thereby allowing the inference of ε across different biomes. For the biomes represented in this study, RMSE= 0.22 $gCMJ^{-1}$.

The simultaneous acquisition of PRI and α_s from multi-angular satellite imagery allowed, for the first time, a spatially explicit mapping of ε in those areas common to all multi-angular images acquired during one overpass. Figure 8A-F shows the spatial distribution of an instantaneous value of ε. The location of the flux-tower is shown in each map (please note that three southern Boreas sites (OJP, HJP 1975, and HJP 2002) were all contained in the same CHRIS/Proba acquisition (Figure D)). The spatial variation across the different sites is clearly visible in Figure 8. Variations in ε were more pronounced at the denser coniferous sites (Figures A, C), than at the deciduous stands (Figure B). The largest differences in ε were found at the Tumbarumba site (E). High light-use efficiencies were observed for the irrigated pasture land (North-West), but low productivity was predicted for the non-irrigated, forested sites. The smallest variability of all sites was observed at the NOBS site.

5. Discussion

This study has demonstrated the observation of vegetation ε and therefore photosynthesis in a spatially continuous mode from satellite observations. The results reported in here are also supported by theoretical work using radiative transfer theory [*Hall et al.*, 2011; *Hall et al.*, 2008] and stand level optical data collected continuously over three years. *Hilker et al.*, [2010] compared multi-angular tower-based radiometer data acquired at the DF-49 site and a mature Aspen stand in central Saskatchewan and found the regression lines between PRI' and ε of both stands to fall within the 95% confidence interval of each other. While the relationship derived in *Hilker et al.*, [2010, Fig. 10] is very similar to the one presented in this study, both are not directly comparable because of 1) atmospheric effects, which have not been accounted for in this study and 2) the different ways in which α_s was determined.

CHRIS/Proba is currently the only sensor in orbit that allows multi-angular acquisitions of the PRI wavebands along-track, that is, during one overpass. Previous studies have demonstrated that other

sensors, including NASA's Moderate Resolution Imaging Spectroradiometer (MODIS) are also able to obtain xanthophyll sensitive measurements from different view angles [*Drolet et al.*, 2005; *Drolet et al.*, 2008; *Hilker et al.*, 2009]. However, a multi-angular capability from MODIS is not possible during a single overpass, rendering the computation of ΔPRI $\Delta\alpha_s^{-1}$ impossible.

While this study has successfully used CHRIS/Proba to infer stand-level ε across a range of forested vegetation types, the limitations of this sensor are also acknowledged. First, while the geo-registration algorithm applied in this study yielded sufficiently accurate results to infer PRI and α_s from stacks of multi-angular acquisitions (Figure 3), more sophisticated models will likely be required at least in mountainous and more rugged terrains [*Ma et al.*, 2010]. One such approach could be a rigorous orthorectification technique [*Toutin et al.*, 1992], but further research will be required to allow the application of such an approach in an automated fashion. Second, an appropriate atmospheric correction algorithm will be needed to account for the anisotropy of PRI reflectance and increase the observation accuracy of spaceborne measurements. One such algorithm that has yielded promising results for MODIS data is the multi-angular implementation of atmospheric correction [*Lyapustin and Wang*, 2009], however, adaptations will be necessary to allow the correction of finer spatial resolution (<100 m) along track observations obtained from CHRIS.

Being a demonstration instrument, CHRIS/Proba does not provide global coverage and data is limited to a few predefined locations, as the sensor was not designed to acquire and disseminate data on a regular schedule. As a result, the acquisition of spatially-contiguous, high temporal frequency epsilon measurements desired to improve global GPP estimates, would require a new mission design. *Hall et al.*, [2011] proposed a new, light-weight satellite platform to allow simultaneous acquisitions of f_{par} , PAR, and ε on a spatially contiguous basis at regular time intervals from space. The mission permit a nearly simultaneous acquisition of PRI and NDVI wavebands from 5 angles and at a wide swath to allow global coverage with high temporal (daily) and moderate spatial (90 m) resolution.

One of the advantages of PRI' rather than PRI is that PRI' is independent of extraneous effects (Figure 7). Hall et al 2008, 2011 and Hilker et al. 2010 have shown theoretically and demonstrated experimentally that

1) Non-photosynthetic canopy elements do not contribute to PRI', because photosynthetic down regulation does not affect the PRI of non-photosynthesizing canopy elements.

2) The measured differences in PRI between the sunlit and shaded photosynthetically active elements of the canopy are driven almost exclusively by the difference in ε, hence PRI.

3) The relationship between PRI' and ε is largely independent of changes in canopy chemistry, e.g. the chlorophyll/carotenoid ratio [*Stylinski et al.,* 2002], because PRI' is insensitive to the unstressed leaf reflectance.

While CHRIS/Proba cannot be used in an operational sense, this satellite platform provides a unique opportunity to further test and develop the technique described in this study. Additional research is needed to investigate the use of PRI' across additional forested ecosystems, particularly the tropics, as well as non-forested vegetation types. Such sites could pose new challenges as the variability in shadow fractions is likely reduced due to a lack of structure. Likewise, the application of our approach to more heterogeneous stands also requires additional evaluation. An important aspect of satellite remote sensing of ε is that these observations will be skewed towards conditions where canopy epsilon is low, because they can only be acquired during sunny. The potential implications for integrating sunny and cloudy periods across range of sky diffuse fraction values in a modelling context need to be assessed in future research. An additional aspect for future research is to develop the science measurement and system design requirements for a space mission. Such missions may, for instance, benefit from observations acquired during the morning or later afternoon hours to facilitate the investigation of diurnal cycles and short term vegetation responses.

Global observation of GEP should significantly improve existing productivity and Earth system models [*Goetz and Prince*, 1998, *Running et al*., 2000 *Potter et al.,* 1993, *Sellers et al.,* 1994, 1995] by providing the observations needed to both improve model biophysics, calibration and error assessment. For instance, PRI' observations could be used in a data assimilation approach to frequently assess and potentially correct the performance of vegetation growth models in a spatially explicit fashion. In addition, estimation of ε from PRI' will also help in understanding stress behaviour in plants at the landscape level, thereby predicting ecosystem responses to a changing environment [*Sellers*, 1985].

Conclusion

We have shown that along any orbital track, ε can be inferred from $\Delta\alpha_s\Delta PRI^{-1}$ with a logarithmic relationship across a wide assortment of forested biomes. The CHRIS/Proba sensor provides a unique basis for further research. Ultimately a new space mission could infer PRI' at high temporal resolution globally, in a spatially contiguous mode. Adding additional spectral bands, such as the near infrared and red wavelengths, to such a satellite sensor to measure f_{PAR} would provide a direct estimate of GEP. We conclude that a new sensor design with the desired spatial coverage and revisit frequency to derive f_{PAR} and ε from multiple angles would allow up to daily observations of photosynthesis from space.

Acknowledgements

The ESA CHRIS/Proba images were provided by Dr. David G. Goodenough, Dr. Ray Merton, and Dr. Mathias Kneubühler, all principal investigators of the Evaluation and Validation of CHRIS (EVC) Project. This research is partially funded by the Canadian Carbon Program, the Natural Sciences and Engineering Research Council of Canada (NSERC) and BIOCAP, and an NSERC-Accelerator grant to NCC.

References

Amiro, B. D., et al. (2006), Carbon, energy and water fluxes at mature and disturbed forest sites, Saskatchewan, Canada, *Agricultural and Forest Meteorology*, *136*(3-4), 237-251.

Baldocchi, D., et al. (2001), Fluxnet: a New Tool to Study the Temporal and Spatial Variability of Ecosystem-Scale Carbon Dioxide, Water Vapor, and Energy Flux Densities, *Bulletin of the American Meteorological Society*, *82*(11), 2415-2434.

Barr, A. G., T. A. Black, E. H. Hogg, N. Kljun, K. Morgenstern, and Z. Nesic (2004), Inter-annual variability in the leaf area index of a boreal aspen-hazelnut forest in relation to net ecosystem production, *Agricultural and Forest Meteorology*, *126*(3-4), 237-255.

Bergeron, O., H. A. Margolis, T. A. Black, C. Coursolle, A. L. Dunn, A. G. Barr, and S. C. Wofsy (2007), Comparison of carbon dioxide fluxes over three boreal black spruce forests in Canada, *Global Change Biology*, *13*(1), 89-107.

Black, T. A., et al. (1996), Annual Cycles of Water Vapour and Carbon Dioxide Fluxes in and Above a Boreal Aspen Forest, *Global Change Biology*, *2*(3), 219-229.

Chen, J. M. (1996), Canopy Architecture and Remote Sensing of the Fraction of Photosynthetically Active Radiation Absorbed by Boreal Conifer Forests, *Ieee Transactions on Geoscience and Remote Sensing*, *34*(6), 1353-1368.

Chen, J. M., A. Govind, O. Sonnentag, Y. Q. Zhang, A. Barr, and B. D. Amiro (2006), Leaf Area Index Measurements at Fluxnet-Canada Forest Sites, *Agricultural and Forest Meteorology*, *140*, 257-268.

Coops, N. C., T. Hilker, F. G. Hall, C. J. Nichol, and G. G. Drolet (2010), Estimation of Light-use Efficiency of Terrestrial Ecosystem from Space: A Status Report, *Bioscience*, *60*(10), 788-797.

Demmig- Adams, B., and W. W. Adams (1996), The Role of Xanthophyll Cycle Carotenoids in the Protection of Photosynthesis, *Trends in Plant Science*, *1*(1), 21-26.

Demmig-Adams, B. (1998), Survey of Thermal Energy Dissipation and Pigment Composition in Sun and Shade Leaves, *Plant and Cell Physiology*, *39*(5), 474-482.

Drolet, G. G., K. F. Huemmrich, F. G. Hall, E. M. Middleton, T. A. Black, A. G. Barr, and H. A. Margolis (2005), A Modis-Derived Photochemical Reflectance Index to Detect Inter-Annual Variations in the Photosynthetic Light-Use Efficiency of a Boreal Deciduous Forest, *Remote Sensing of Environment*, *98*(2-3), 212-224.

Drolet, G. G., E. M. Middleton, K. F. Huemmrich, F. G. Hall, B. D. Amiro, A. G. Barr, T. A. Black, H. A. mcCaughey, and H. A. Margolis (2008), Regional mapping of gross light-use efficiency using MODIS spectral indices, *Remote Sensing of Environment*, *112*, 3064-3078.

Fletcher, P.A. (2004), Image acquisition planning for the CHRIS sensor onboard PROBA. *Proceedings of SPIE, the international society for optical engineering, 5546,* 141-148.

Fuentes, D. A., J. A. Gamon, Y. F. Cheng, H. C. Claudio, H. L. Qiu, Z. Y. Mao, D. A. Sims, A. F. Rahman, W. Oechel, and H. Y. Luo (2006), Mapping carbon and water vapor fluxes in a chaparral ecosystem using vegetation indices derived from AVIRIS, *Remote Sensing of Environment*, *103*(3), 312-323.

Gamon, J. A., J. Penuelas, and C. B. Field (1992), A Narrow-Waveband Spectral Index That Tracks Diurnal Changes in Photosynthetic Efficiency, *Remote Sensing of Environment*, *41*(1), 35-44.

Gamon, J. A., L. Serrano, and J. S. Surfus (1997), The Photochemical Reflectance Index: an Optical Indicator of Photosynthetic Radiation Use Efficiency Across Species, Functional Types, and Nutrient Levels, *Oecologia*, *112*(4), 492-501.

Goetz, S. J., and S. D. Prince (1998), Variability in Carbon Exchange and Light Utilization Among Boreal Forest Stands: Implications for Remote Sensing of Net Primary Production, *Canadian Journal of Forest Research-Revue Canadienne De Recherche Forestiere*, *28*(3), 375-389.

Gomez-Chova, L., L. Alonso, L. Guanter, G. Camps-Valls, J. Calpe, and J. Moreno (2008), Correction of systematic spatial noise in push-broom hyperspectral sensors: application to CHRIS/PROBA images, *Applied Optics*, *47*(28), F46-F60.

Goshtasby, A. (1988), IMAGE REGISTRATION BY LOCAL APPROXIMATION METHODS, *Image and Vision Computing*, *6*(4), 255-261.

Goulden, M. L., and P. M. Crill (1997), Automated Measurements of Co2 Exchange at the Moss Surface of a Black Spruce Forest, *Tree Physiology*, *17*(8-9), 537-542.

Gruninger, J., A. J. Ratkowski, and M. L. Hoke (2004), The sequential maximum angle convex cone (SMACC) endmember model, *Algorithms and Technologies for Multispectral, Hyperspectral, and Ultraspectral Imagery X*, *5425*, 1-14.

Hall, F.G., D.E. Knapp and K.F. Huemmrich, 1997. Physically based classification and satellite mapping of biophysical characteristics in the southern boreal forest, Journal of Geophysical Research,. 102, NO. D24, PAGES 29,567-29,580, DECEMBER 26, 1997

Hall, F. G., D. R. Peddle, and E. F. Ledrew (1996), Remote sensing of biophysical variables in boreal forest stands of Picea mariana, *International Journal of Remote Sensing*, *17*(15), 3077-3081.

Hall, F.G., Y.E. Shimabukuro, 1995. Remote Sensing of Forest Biophysical Structure using Mixture Decomposition and Geometric Reflectance Models, Ecological Applications, 5(4), pp 993-1013.

Hall, F. G., T. Hilker, and N. C. Coops (2011), PHOTOSYNSAT, Photosynthesis from space: Theoretical foundations of a satellite concept and validation from tower and spaceborne data, *Remote Sensing of Environment*, *in press.* doi:10.1016/j.rse.2011.03.014

Hall, F. G., T. Hilker, N. C. Coops, A. Lyapustin, K. F. Huemmrich, E. Middleton, H. Margolis, G. Drolet, and T. A. Black (2008), Multi-angle remote sensing of forest light use efficiency by observing PRI variation with canopy shadow fraction, *Remote Sensing of Environment*, *112*(7), 3201-3211.

Hilker, T., N. C. Coops, M. A. Wulder, T. A. Black, and R. D. Guy (2008a), The use of remote sensing in light use efficiency based models of gross primary production: A review of current status and future requirements, *Science of the Total Environment*, *404*(2-3), 411-423.

Hilker, T., N. C. Coops, C. R. Schwalm, R. S. Jassal, T. A. Black, and P. Krishnan (2008b), Effects of mutual shading of tree crowns on prediction of photosynthetic light-use efficiency in a coastal Douglas-fir forest, *Tree Physiology*, *28*(6), 825-834.

Hilker, T., N. C. Coops, F. G. Hall, T. A. Black, M. A. Wulder, Z. Nesic, and P. Krishnan (2008c), Separating physiologically and directionally induced changes in PRI using BRDF models, *Remote Sensing of Environment*, *112*(6), 2777-2788.

Hilker, T., A. Lyapustin, F. G. Hall, Y. Wang, N. C. Coops, G. Drolet, and T. A. Black (2009), An assessment of photosynthetic light use efficiency from space: Modeling the atmospheric and directional impacts on PRI reflectance, *Remote Sensing of Environment*, *113*(11), 2463-2475.

Hilker, T., et al. (2010), Remote sensing of photosynthetic light-use efficiency across two forested biomes: Spatial scaling, *Remote Sensing of Environment*, *114*, 2863–2874.

Horii, C. V., J. W. Munger, S. C. Wofsy, M. Zahniser, D. Nelson, and J. B. McManus (2004), Fluxes of nitrogen oxides over a temperate deciduous forest, *Journal of Geophysical Research-Atmospheres*, *109*(D8).

Humphreys, E. R., T. A. Black, K. Morgenstern, T. B. Cai, G. B. Drewitt, Z. Nesic, and J. A. Trofymow (2006), Carbon Dioxide Fluxes in Coastal Douglas-Fir Stands at Different Stages of Development After Clearcut Harvesting, *Agricultural and Forest Meteorology*, *140*(1-4), 6-22.

Leprince, S., S. Barbot, F. Ayoub, and J. P. Avouac (2007), Automatic and precise orthorectification, coregistration, and subpixel correlation of satellite images, application to ground deformation measurements, *Ieee Transactions on Geoscience and Remote Sensing*, *45*(6), 1529-1558.

Leuning, R., H. A. Cleugh, S. J. Zegelin, and D. Hughes (2005), Carbon and water fluxes over a temperate Eucalyptus forest and a tropical wet/dry savanna in Australia: measurements and comparison with MODIS remote sensing estimates, *Agricultural and Forest Meteorology*, *129*(3-4), 151-173.

Lowe, D. G. (2004), Distinctive image features from scale-invariant keypoints, *International Journal of Computer Vision*, *60*(2), 91-110.

Lyapustin, A., and Y. Wang (2009), *The time series technique for aerosol retrievals overland from MODIS*, Springer Praxis Books 978-3-540-69396-3., Berlin.

Lyapustin, A., Y. Wang, R. Kahn, J. Xiong, A. Ignatov, R. Wolfe, A. Wu, B. Holben, and C. Bruegge (2007), Analysis of MODIS-MISR calibration differences using surface albedo around AERONET sites and cloud reflectance, *Remote Sensing of Environment*, *107*(1-2), 12-21.

Nakaji, T., Oguma, H., & Fujinuma, Y. (2006), Seasonal changes in the relationship between photochemical reflectance index and photosynthetic light use efficiency of Japanese larch needles. *International Journal of Remote Sensing*, 27, 493−509.

Nichol, C.J., Huemmrich, K.F., Black, T.A., Jarvis, P.G., Walthall, C.L., Grace, J., Hall, F.G., 2000. Remote Sensing of Photosynthetic-Light-Use Efficiency of Boreal Forest. *Agricultural and Forest Meteorology* 101, 131-142

Ma, J. L., J. C. W. Chan, and F. Canters (2010), Fully Automatic Subpixel Image Registration of Multiangle CHRIS/Proba Data, *Ieee Transactions on Geoscience and Remote Sensing*, *48*(7), 2829-2839.

Meroni, M., M. Rossini, V. Picchi, C. Panigada, S. Cogliati, C. Nali, and R. Colombo (2008), Assessing steady-state fluorescence and PRI from hyperspectral proximal sensing as early indicators of plant stress: The case of ozone exposure, *Sensors*, *8*(3), 1740-1754.

Monteith, J. L. (1972), Solar-Radiation and Productivity in Tropical Ecosystems, *Journal of Applied Ecology*, *9*(3), 747-766.

Monteith, J. L. (1977), Climate and Efficiency of Crop Production in Britain, *Philosophical Transactions of the Royal Society of London Series B-Biological Sciences*, *281*(980), 277-294.

Morgenstern, K., T. A. Black, E. R. Humphreys, T. J. Griffis, G. B. Drewitt, T. B. Cai, Z. Nesic, D. L. Spittlehouse, and N. J. Livingstone (2004), Sensitivity and Uncertainty of the Carbon Balance of a Pacific Northwest Douglas-Fir Forest During an El Nino La Nina Cycle, *Agricultural and Forest Meteorology*, *123*(3-4), 201-219.

Myneni, R. B., and D. L. Williams (1994), On the Relationship Between Fapar and Ndvi, *Remote Sensing of Environment*, *49*(3), 200-211.

Peddle, D. R., and A. M. Smith (2005), Spectral mixture analysis of agricultural crops: endmember validation and biophysical estimation in potato plots, *International Journal of Remote Sensing*, *26*(22), 4959-4979.

Potter, C.S., Randerson, J.T., Field, C.B., Matson, P.A., Vitousek, P.M., Mooney, H.A., Klooster, S.A., 1993. Terrestrial Ecosystem Production - a Process Model-Based on Global Satellite and Surface Data. *Global Biogeochemical Cycles* 7, 811-841

Rahman, A. F., J. A. Gamon, D. A. Fuentes, D. A. Roberts, and D. Prentiss (2001), Modeling Spatially Distributed Ecosystem Flux of Boreal Forest Using Hyperspectral Indices From Aviris Imagery, *Journal of Geophysical Research-Atmospheres*, *106*(D24), 33579-33591.

Running, S., Baldocchi, D., Turner, D., Gower, S., Bakwin, P., Hibbard, K., 1999. A global terrestrial monitoring network integrating tower fluxes, flask sampling, ecosystem modeling and EOSD satellite data. *Remote Sensing of Environment* 70, 108-127

Schwalm, C. R., et al. (2006), Photosynthetic Light Use Efficiency of Three Biomes Across an East-West Continental-Scale Transect in Canada, *Agricultural and Forest Meteorology*, *140*(1-4), 269-286.

Sellers, P. J. (1985), Canopy Reflectance, Photosynthesis and Transpiration, *International Journal of Remote Sensing*, *6*(8), 1335-1372.

Sellers, P. J., C. J. Tucker, G. J. Collatz, S. O. Los, C. O. Justice, D. A. Dazlich, and D. A. Randall (1994), A Global 1-Degrees-by-1-Degrees Ndvi Data Set for Climate Studies .2. The Generation of Global Fields of Terrestrial Biophysical Parameters From the Ndvi, *International Journal of Remote Sensing*, *15*(17), 3519-3545.

Sellers, P.J., Meeson, B.W., Hall, F.G., Asrar, G., Murphy, R.E., Schiffer, R.A., Bretherton, F.P., Dickinson, R.E., Ellingson, R.G., Field, C.B., Huemmrich, K.F., Justice, C.O., Melack, J.M., Roulet, N.T., Schimel, D.S., Try, P.D., 1995. Remote-Sensing of the Land-Surface for Studies of Global Change - Models, Algorithms, Experiments. *Remote Sensing of Environment* 51, 3-26

Shaker, A., J. E. Nichol, and M. S. Wong (2008), Potential accuracy of image orientation of small satellites: A case study of CHRIS/Proba data, *Photogrammetric Record*, *23*(123), 275-289.

Staebler, R. M., and D. R. Fitzjarrald (2005), Measuring canopy structure and the kinematics of subcanopy flows in two forests, *Journal of Applied Meteorology*, *44*(8), 1161-1179.

Stylinski, C. D., Gamon, J. A., & Oechel, W. C. (2002), Seasonal patterns of reflectance indices, carotenoid pigments and photosynthesis of evergreen chaparral species. *Oecologia*, 131, 366−374.

Thuillier, G., M. Herse, D. Labs, T. Foujols, W. Peetermans, D. Gillotay, P. C. Simon, and H. Mandel (2003), The solar spectral irradiance from 200 to 2400 nm as measured by the SOLSPEC spectrometer from the ATLAS and EURECA missions, *Solar Physics*, *214*(1), 1-22.

Toutin, T. (2004), Review article: Geometric processing of remote sensing images: models, algorithms and methods, *International Journal of Remote Sensing*, *25*(10), 1893-1924.

Toutin, T., Y. Carbonneau, and L. St-Laurent (1992), An integrated method to rectify airborne radar imagery using DEM, *Photogrammetric Engineering & Remote Sensing*, *58*(4), 417-422.

Valentini, R., et al. (2000), Respiration as the Main Determinant of Carbon Balance in European Forests, *Nature*, *404*(6780), 861-865.

Van Laake, P. E., and G. A. Sanchez-Azofeifa (2005), Mapping Par Using Modis Atmosphere Products, *Remote Sensing of Environment*, *94*(4), 554-563.

Xiao, X. M., Q. Y. Zhang, D. Hollinger, J. Aber, and B. Moore (2005), Modeling gross primary production of an evergreen needleleaf forest using modis and climate data, *Ecological Applications*, *15*(3), 954-969.

Tables

Table 1: Site description

Site, Reference	Lat (°)/ Long (°)	Elev. (m)	Dominant Species	Leaf Area Index	Age (years)	Height (m)	Annual mean temp. (°C)
DF-49 [*Morgenstern et al.*, 2004]	-125.334 49.867	340	*Pseudotsuga menziesii, Thuja plicata, Tsuga heterophylla*	7.1	60	35	8.1
Harvard [*Staebler and Fitzjarrald*, 2005]	-72.171 42.537	340	*Quercus rubra, Acer rubrum, Betula lenta, Pinus strobes, Tsuga Canadensis*	3.4	80	23	8.3
HJP1975 [*Amiro et al.*, 2006; *J.M. Chen et al.*, 2006; *Schwalm et al.*, 2006]	-104.645 53.876	570	*Pinus banksiana*	1.4	35	6	0.4
HJP2002 [*Amiro et al.*, 2006; *J.M. Chen et al.*, 2006; *Schwalm et al.*, 2006]	-104.649 53.908	560	*Pinus banksiana*	0.9	8	0.1	0.4
Howland[*Xiao et al.*, 2005]	-68.740 45.204	60	*Pinus rubens, Tsuga canadensis*	5.3	109	20	6.7
NOBS [*Bergeron et al.*, 2007]	-98.481 55.880	259	*Picea mariana*	4.8	160	9	-4.4
OJP[*Amiro et al.*, 2006; *J.M. Chen et al.*, 2006; *Schwalm et al.*, 2006]	-104.692 53.916	579	*Pinus banksiana*	2	91	13	0.4
Tumbarumba [*Leuning et al.*, 2005]	148.152 -35.656	1000	*Eucalyptus delegatensis, Eucalyptus dalrymplean*	1.4	90	40	8.0

Figures

Figure 1: Location of the selected research sites. CHRIS/Proba and eddy-flux data were collected simultaneously between the years 2002 and 2008

Figure 2: Structural differences at the 8 research sites presented in this study. The sites are DF-49 (A), Harvard Forest (B), HJP1975(C), HJP2002 (D), Howland Forest (E), NOBS (F), OJP (G) and Tumbarumba (H)

Figure 3: Acquisition of ΔPRI $\Delta\alpha_s^{-1}$ for a given CHRIS/Proba overpass. PRI values and corresponding shadow fractions were obtained for each pixel of a stack of up to 5 multi-angular observations acquired along track under conditions where stand level ε can assumed to be constant.

Figure 4: Range of variability in ε across the eight different test sites during the CHRIS/Proba overpasses. All of these observations have been acquired at different times of the day during the satellite overpasses and are not representative of the physiological conditions of each stand (Number of cloud free observations: Df-49: n=9, Harvard Forest: n=3, HJP1975: n=8, HJP2002: n=8 and OJP: n=8, Howland Forest: n=10, Tumbarumba: n=3, NOBS: n=3).

Figure 5: Boxplot of the coefficient of determination (r^2) for the relationship between PRI and α_s across all sites grouped into different levels of EC-measured ε. Strong linear relationships were found for low levels of ε, but the relationship weakened for higher ε as PRI became less driven by canopy shadow fractions (Number of observations: n=6 (ε <0.05), n=17 (0.05<ε <0.15), n=18 (0.15<ε <0.25), n=10 (ε >0.25))

Figure 6: A-D: Slope between PRI and α_s for four different levels of ε, here using HJP1975 as an example. Figure E-H illustrates the corresponding environmental conditions including PAR, GEP, pressure

deficit (D) and temperature (T) for the ε values presented in A-D. The relationship between PRI and α_s begins to disintegrate as ε approaches ε_{max}.

Figure 7: Relationship between ΔPRI $\Delta\alpha_s^{-1}$ (PRI') as observed from CHRIS/Proba imagery and EC measured ε for eight different research sites. The observations have been taken between 2001 and 2009.

Figure 8: Maps of ε (in $gCMJ^{-1}$) as estimated from CHRIS/Proba imagery using the relationship shown in Figure 7. The spatial variability in ε is apparent at all sites. At the Australian site, ε is also driven by availability of water, as the irrigated pasture shows significantly higher ε than the surrounding forest.

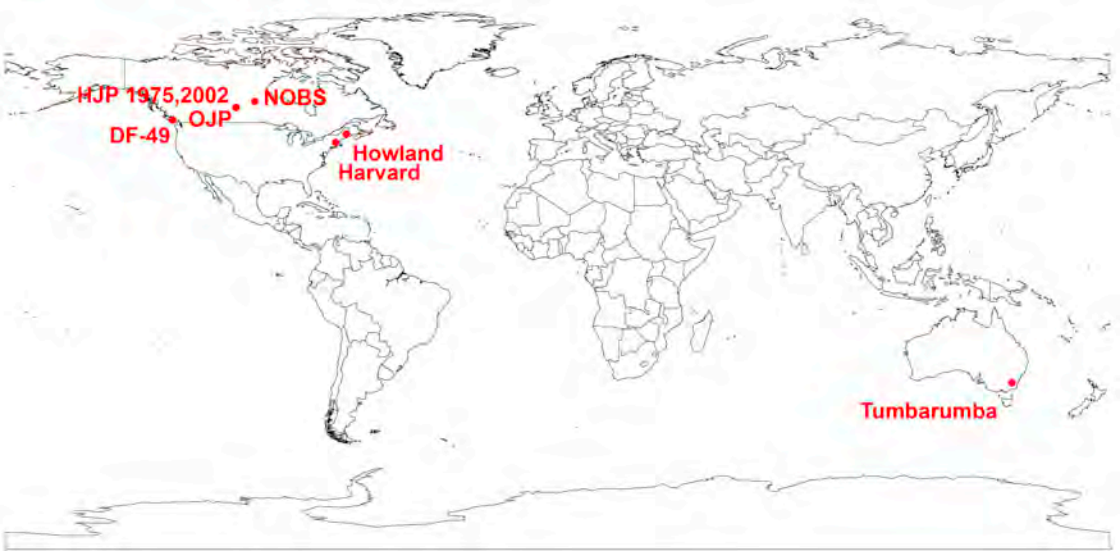
HJP 1975,2002
NOBS
OJP
DF-49
Howland
Harvard
Tumbarumba

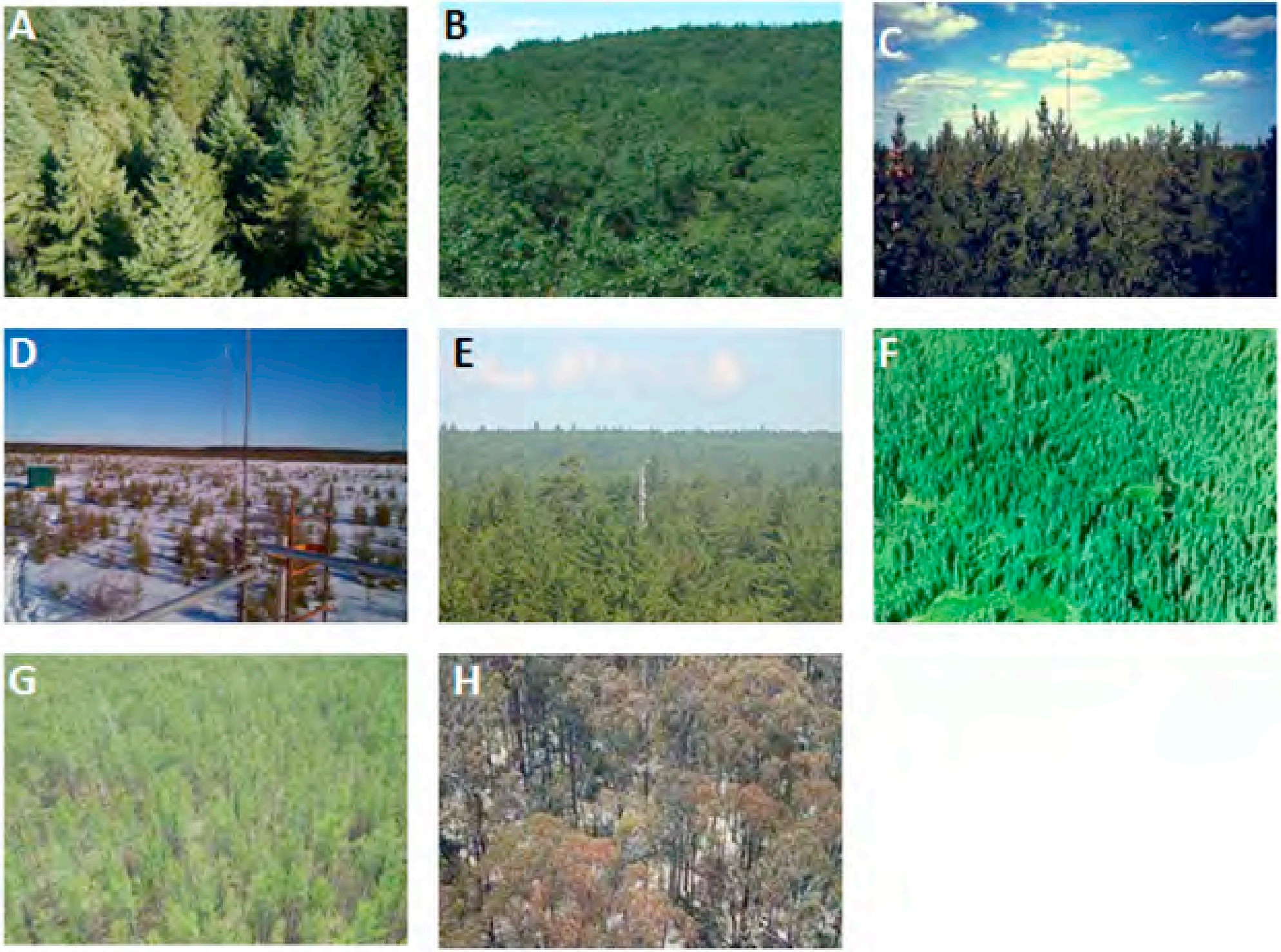
A
B
C
D
E
F
G
H

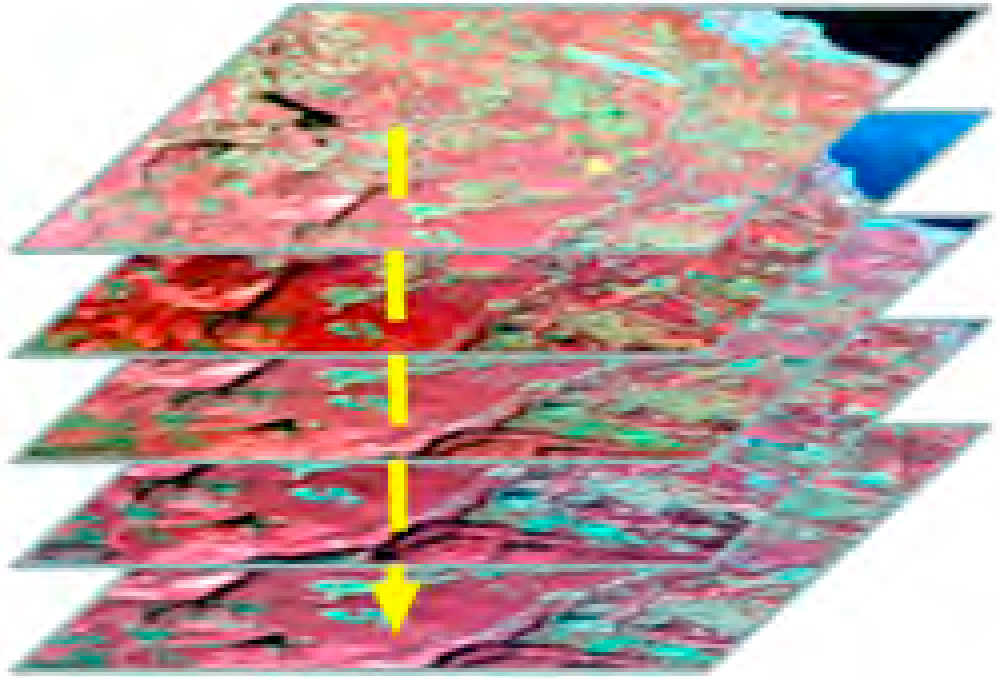

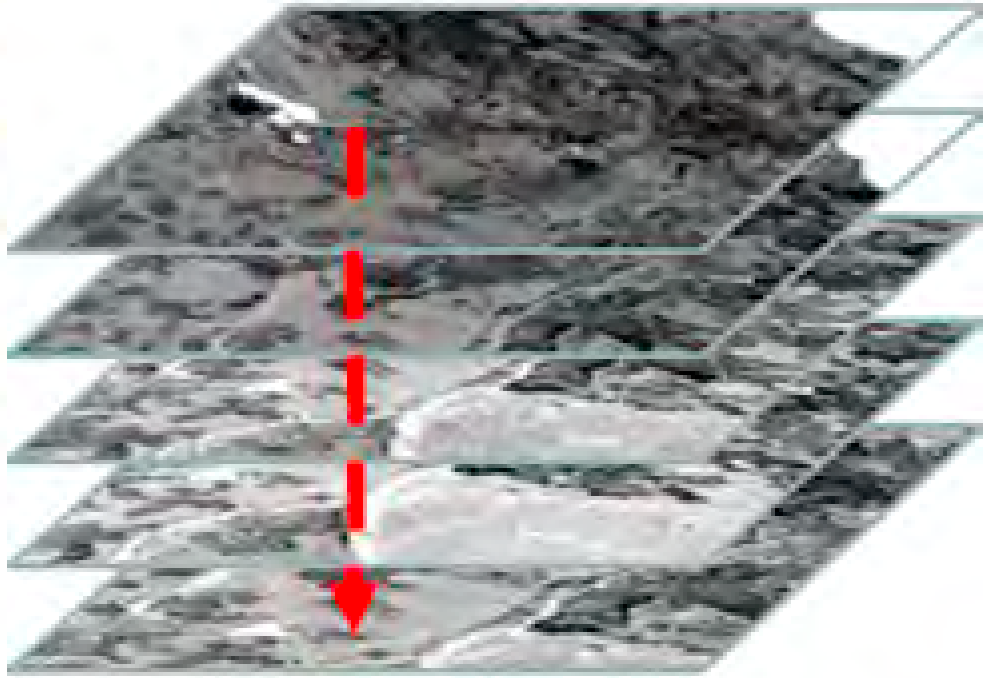

Reflectance for given overpass

Corresponding Shadow fractions from spectral endmembers

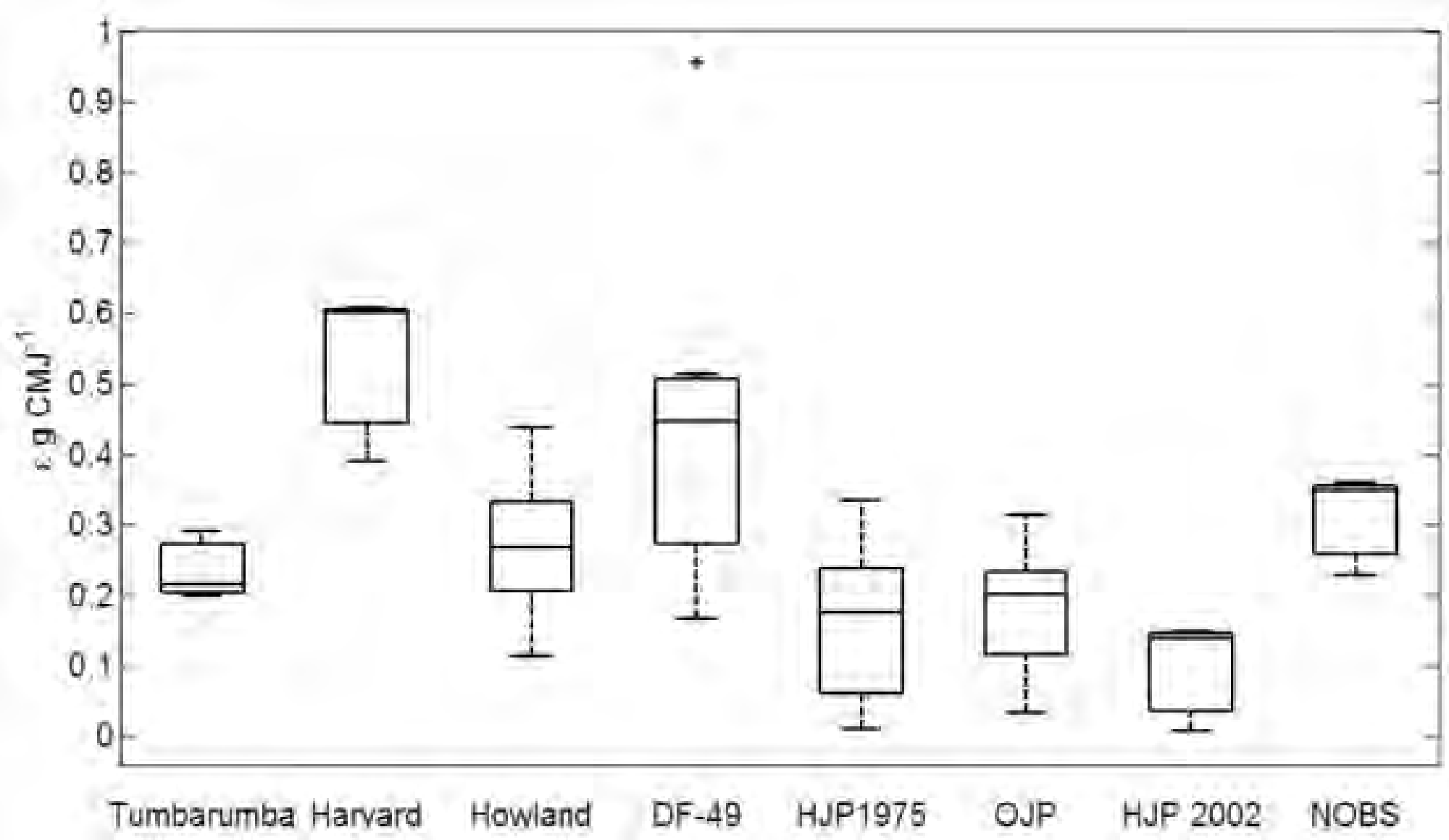
1
0.9
0.8
0.7
0.6
0.5
0.4
0.3
0.2
0.1
0
ε g CMJ⁻¹
Tumbarumba
Harvard
Howland
DF-49
HJP1975
OJP
HJP 2002
NOBS

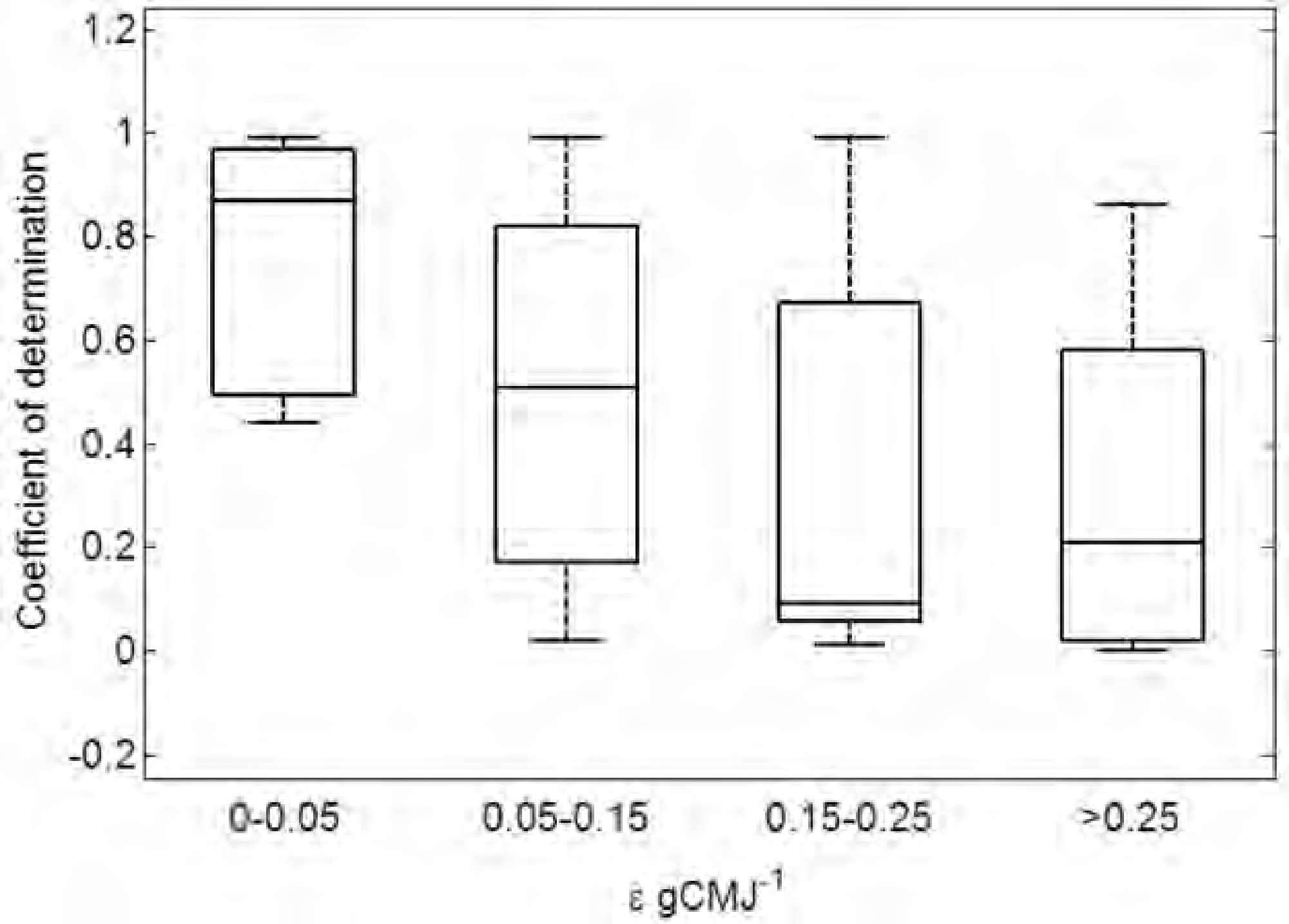
Coefficient of determination
1.2
1
0.8
0.6
0.4
0.2
0
-0.2
0-0.05
0.05-0.15
0.15-0.25
>0.25
ε gCMJ-1

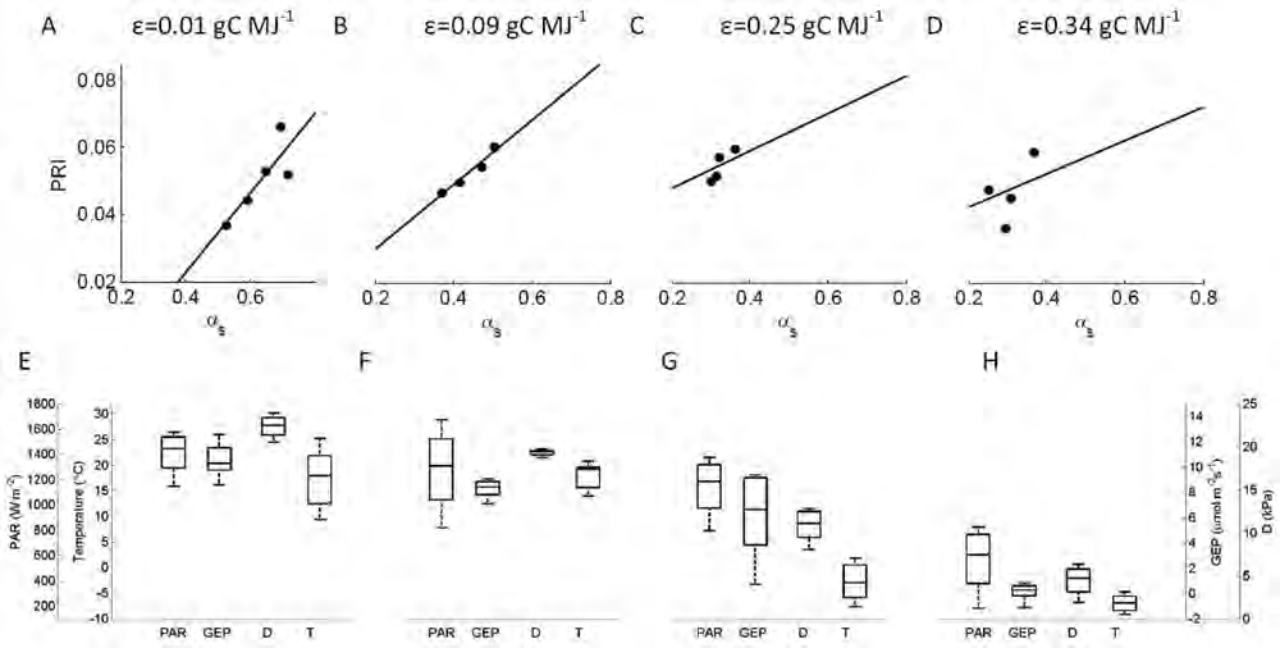
A
ε=0.01 gC MJ-1
B
ε=0.09 gC MJ-1
C
ε=0.25 gC MJ-1
D
ε=0.34 gC MJ-1
PRI
0.08
0.06
0.04
0.02
0.2
0.4
0.6
0.8
αs
E
F
G
H
PAR (W/m-2)
Temperature (°C)
GEP (µmol m-2s-1)
D (kPa)
PAR
GEP
D
T

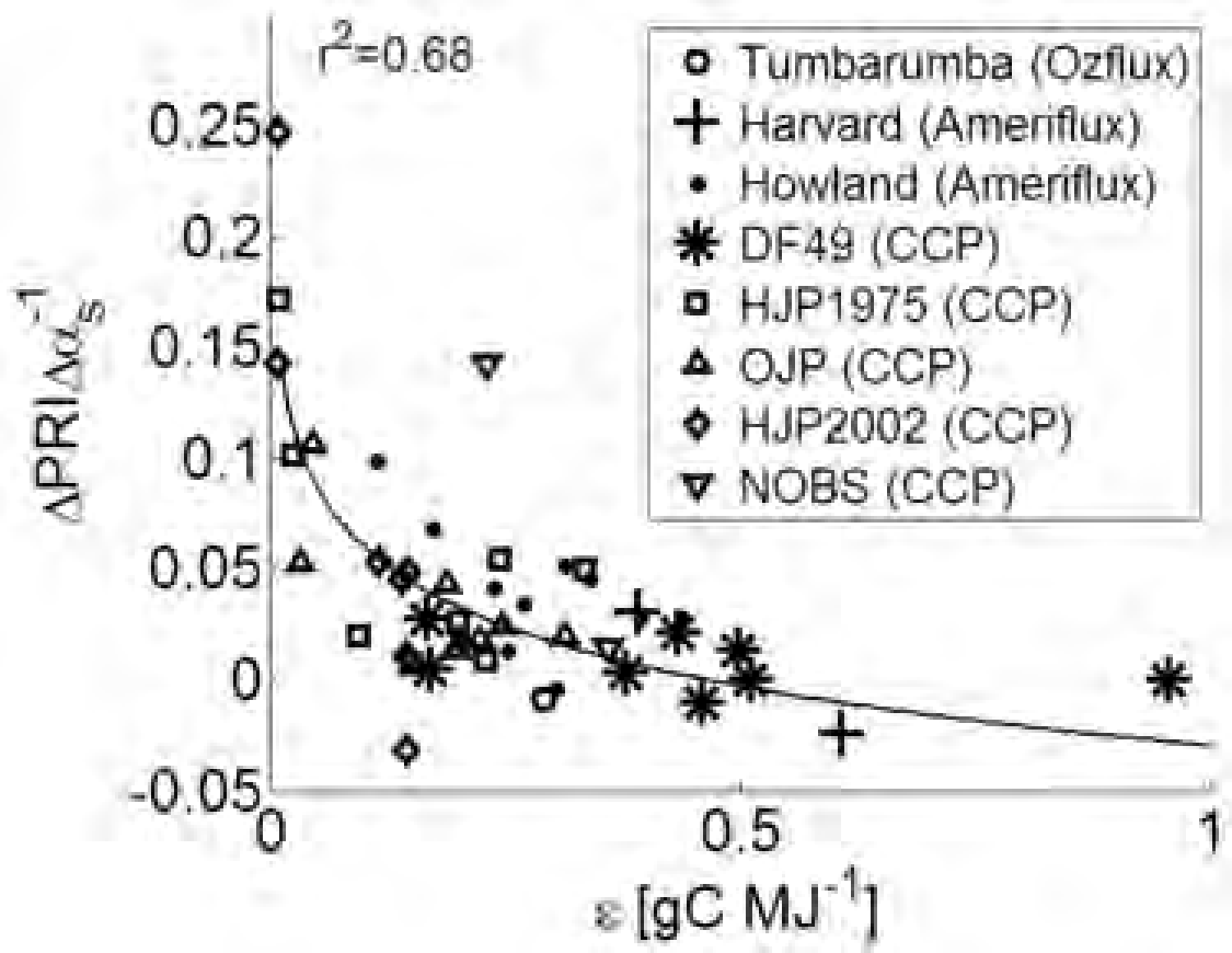
r^2=0.68
Tumbarumba (Ozflux)
Harvard (Ameriflux)
Howland (Ameriflux)
DF49 (CCP)
HJP1975 (CCP)
OJP (CCP)
HJP2002 (CCP)
NOBS (CCP)
0.25
0.2
0.15
0.1
0.05
0
-0.05
0
0.5
1
$\Delta PRI/\Delta\alpha_s^{-1}$
ε [gC MJ^{-1}]

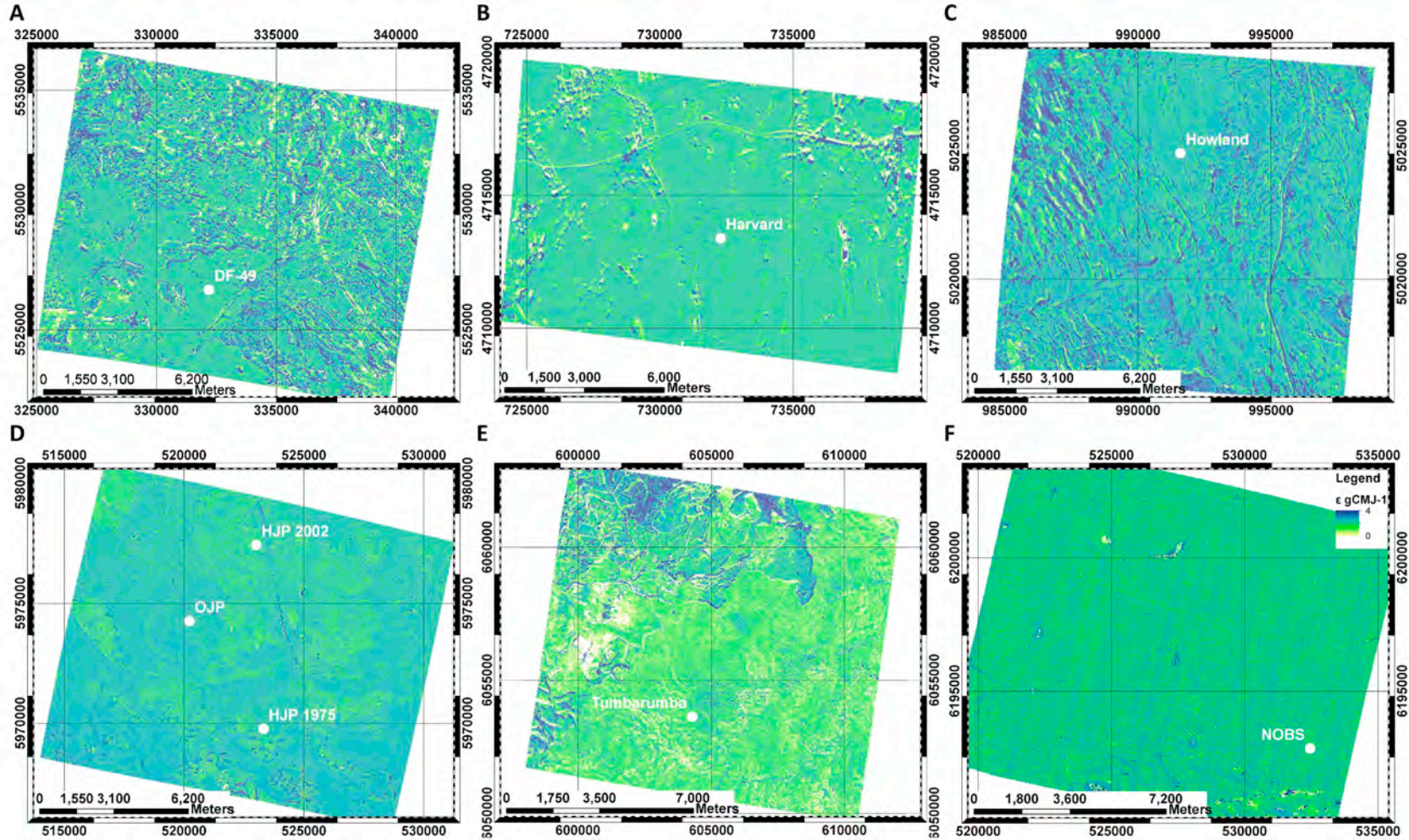
A
325000
330000
335000
340000
5535000
5530000
5525000
DF-49
0 1,550 3,100 6,200
Meters
B
725000
730000
735000
4720000
4715000
4710000
Harvard
0 1,500 3,000 6,000
Meters
C
985000
990000
995000
5025000
5020000
Howland
0 1,550 3,100 6,200
Meters
D
515000
520000
525000
530000
5980000
5975000
5970000
HJP 2002
OJP
HJP 1975
0 1,550 3,100 6,200
Meters
E
600000
605000
610000
6060000
6055000
6050000
Tumbarumba
0 1,750 3,500 7,000
Meters
F
520000
525000
530000
535000
6200000
6195000
Legend
ε gCMJ-1
4
0
NOBS
0 1,800 3,600 7,200
Meters